JOURNAL OF THERMOPHYSICS AND HEAT TRANSFER
Vol. 8, No. 1, Jan.–March 1994

Monte Carlo Prediction of Radiative Heat Transfer in Inhomogeneous, Anisotropic, Nongray Media

Jeff T. Farmer*
NASA Langley Research Center, Hampton, Virginia 23665
and
John R. Howell†
University of Texas at Austin, Austin, Texas 78712

A Monte Carlo solution technique has been formulated to predict the radiative heat transfer in three-dimensional, inhomogeneous participating media which exhibit spectrally dependent emission and absorption and anisotropic scattering. Details of the technique and selected numerical sensitivities are discussed. The technique was applied to a problem involving a medium composed of a gas mixture of carbon dioxide and nitrogen and suspended carbon particles. A homogeneous medium was modeled to examine the effect of total pressure and carbon-particle concentration on radiative heat transfer. Variation in total pressure, over the range studied, had minimal effect on the amount of heat radiated to the enclosure walls and on the radiative-flux distribution within the medium. Increases in the carbon particle concentration produced significantly higher heat fluxes at the boundaries and altered the radiative flux distribution. The technique was then applied to an inhomogeneous medium to examine effects of specific temperature and carbon particle concentration distributions on radiative heat transfer. For the inhomogeneous conditions examined, the largest radiative flux divergence occurs near the center of the medium and the regions near some enclosure walls act as energy sinks.

Nomenclature

D = distance traveled prior to scattering event
D_e = distance to exit point from current subregion
$e_{b\eta}$ = spectral black body emissive power, W/m^2/cm^{-1}
f = coefficient of scattering phase function
g = coefficient of scattering phase function
N = carbon particle concentration, particles/m^3
N_0 = reference concentration for inhomogeneous carbon particle distribution, particles/m^3
P_e = pressure broadening parameter
R = random number chosen from uniform distribution
S = geometric length of travel within subregion, m
S_c/δ = mean line intensity to spacing ratio
T = subregion temperature, K
T_0 = reference temperature for inhomogeneous temperature distribution, K
α_p = Planck mean absorption coefficient, m^{-1}
α_η = spectral absorption coefficient, carbon dioxide, m^{-1}
$\alpha_{\eta c}$ = spectral absorption coefficient, carbon particles, m^{-1}
β = pressure parameter for spectral band
η = wave number, cm^{-1}
η_c = reference wave number for a given carbon dioxide absorption band
η_∞ = maximum wave number for spectral integration
κ_η = spectral extinction coefficient, m^{-1}
μ = cosine of the scatter angle
ρ = gas density, kg/m^3
σ_η = spectral scattering coefficient, m^{-1}
$\Phi(\psi)$ = normalized scattering phase function
ψ = scatter angle

Received Aug. 27, 1992; revision received April 12, 1993; accepted for publication April 13, 1993.

*Aerospace Engineer, Advanced Space Concepts Division.
†Professor, Department of Mechanical Engineering. Fellow AIAA.

Introduction

ACCURATE prediction of three-dimensional radiative heat transfer in a participating medium becomes a formidable task when the spectral absorption and anisotropic scattering characteristics of the medium are considered. Further complications arise if the medium has inhomogeneous properties. Many approaches exist for predicting radiative transfer within participating media, but few can easily or efficiently treat all of these complications. One method that can be applied is the Monte Carlo/ray tracing approach, generally discussed in Refs. 1–3.

In the Monte Carlo approach, the radiative transfer is simulated using the calculated movements of a statistically large number of bundles of radiative energy. As each bundle progresses from its initial location, at emission, through the medium, it experiences scattering, and absorption. Upon completion of the simulation, predictions of heat transfer or temperature distribution are determined, based on the averaged behavior of the set of individual energy bundles.

Although the Monte Carlo approach is relatively easy to use to model extremely complex phenomena, its appetite for computer resources and the statistical nature of the results have inhibited its widespread application. Relatively few published efforts exist concerning the application of the Monte Carlo approach to problems of radiative heat transfer within three-dimensional inhomogeneous media with highly spectral, anisotropic behavior. Recently, however, armed with more powerful computers, researchers are beginning to exploit the Monte Carlo method in such problems. For instance, Modest[4] has begun investigating the problems involving media with complex spectral-line behavior, and Subramaniam and Mengüc[5] and Viskanta[6] discuss the Monte Carlo approach applied to anisotropically scattering gray media. This article discusses the development of a Monte Carlo approach to predict the radiative heat transfer within general inhomogeneous media that exhibit both highly spectral and anisotropic scattering behaviors.

The development of this approach and its application to a test medium were conducted as a part of a symposium[7] on the comparison of solution methods for predicting radiative transfer in complex media. Consequently, the medium characteristics discussed in this article were prespecified by the symposium to correspond to a medium consisting of a mixture of carbon dioxide and nitrogen and carbon particles, similar to a gas and soot mixture from a combustion process. Although this article focuses on the Monte Carlo approach and results, occasional references are made to problem constraints and result comparisons from that symposium.

Participating Media Description

The participating media analyzed in this study consisted of a homogeneous one-dimensional slab between two cold, black walls 5-m apart; a homogeneous three-dimensional medium in a rectangular, cold, black enclosure, with dimensions, $W = 2$, $L = 5$, and $H = 3$ m; and an inhomogeneous three-dimensional medium in a rectangular, cold, gray enclosure, with identical dimensions. W, L, H, are the x, y, z dimensions of the enclosure, shown in Fig. 1. Each medium consisted of a mixture of nitrogen and carbon dioxide gases plus varying concentrations of carbon particles. In the homogeneous media the total mixture pressure and temperature were specified to be 1 atm, with a volume fraction of carbon dioxide of 0.21, and 1000 K, respectively. For the one-dimensional medium, a total pressure of 3 atm was also specified. The carbon particles were specified to be of uniform diameter, 30 μ, and in concentrations of 2.0×10^7, 2.0×10^8, and 2.0×10^9 particles per cubic meter. In the inhomogeneous medium the pressure and volume fraction remained uniform and identical to that for the homogeneous medium, however, the temperature and particle concentrations varied over the medium according to Eqs. (1) and (2), respectively:

$$T(x, y, z) = T_0 \left[\left(1 - 2\frac{|x|}{W}\right) \left(1 - 2\frac{|y|}{L}\right) \times \left(1 - 2\frac{|z|}{H}\right) + 1 \right] \quad (1)$$

$$N(x, y, z) = N_0 \left[3\left(1 - 2\frac{|x|}{W}\right) \left(1 - 2\frac{|z|}{H}\right) + 1 \right] \quad (2)$$

T_0 and N_0 were chosen to be 500 K and either 5×10^7 or 5×10^8 particles per cubic meter, respectively.

Spectrally Dependent Radiative Properties

The models describing spectral behavior of the carbon dioxide gas and the carbon particle concentration are specified in Ref. 7 and are described briefly below. The amount of absorption and emission due to carbon dioxide is highly spectral and is modeled using an absorption profile formulation presented by Edwards.[8] In this formulation, Eqs. (3–6) are applied for each of the major spectral absorption bands:

$$\alpha_\eta = \rho \frac{S_c}{\delta} \frac{\sinh\left(\frac{\pi\beta}{2}\right)}{\cosh\left(\frac{\pi\beta}{2}\right) - \cos\left[\frac{2\pi(\eta - \eta_c)}{\delta}\right]} \quad (3)$$

$$\frac{S_c}{\delta} = \frac{C_1}{C_3} \exp[-(a/C_3)|\eta - \eta_c|] \quad (4)$$

$$\beta = \frac{C_2^2 P_e}{4 C_1 C_3} \quad (5)$$

$$\delta = 30 C_3 (T = 100 \text{ K}) \quad (6)$$

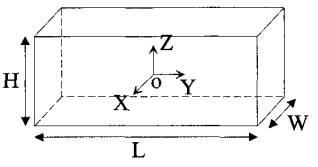

Fig. 1 Coordinate system and dimensions for three-dimensional rectangular media.

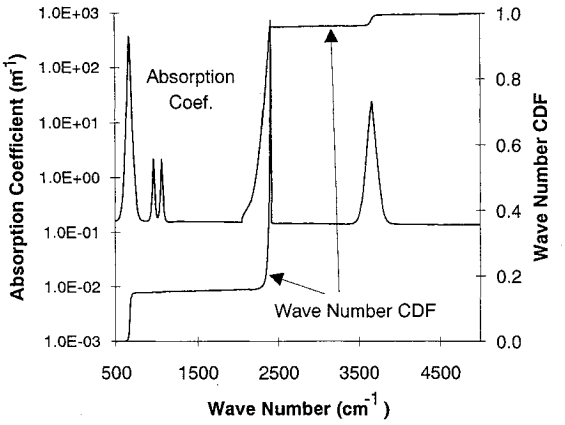

Fig. 2 Combined absorption coefficient and wave number CDF vs wave number for case of gas at $T = 1000$ K, $P = 1$ atm (21% carbon dioxide, by volume), with $N = 2.0\text{E}+08$ particles/m^3.

In this study the five major bands used had η_c of 667, 960, 1060, 2410, and 3660 cm^{-1}. η_c is, essentially, the wave number at the center or peak of each exponentially shaped absorption band. The value of δ, specified in Ref. 7, causes the shape of the absorption profiles to represent the averaged behavior of the absorption line structure within each band, therefore, obscuring the absorption behavior due to the individual line structure. The parameters C_1, C_2, and C_3 are associated with each band and are temperature dependent. The "a" is an asymmetry factor equal to 1 for symmetric bands and 2 for asymmetric bands. The other symbols are briefly described in the Nomenclature and in more detail by Edwards.[8]

The absorption, emission, and scattering due to the carbon particles is directly dependent on the particle size and concentration, and varies slightly with wave number, relative to that of carbon dioxide. For the particle diameter of 30 μ selected for this analysis, the spectral variations in absorption and scattering coefficients are derived from data reported by Foster and Howarth[9] and are listed in Ref. 7. Figure 2 shows the spectral variation in the combined absorption coefficient with wave number for a mixture of carbon dioxide and carbon particles, where the combined absorption is equal to the sum of the absorption due to carbon dioxide and that due to the carbon particles. The gas and particle mixture has a temperature of 1000 K, a total pressure of 1 atm (0.21 volume fraction of carbon dioxide) and a carbon particle concentration of 2×10^8 particles/m^3.

Anisotropic Scattering

The carbon particles exhibit highly forward scattering behavior. Reference 7 specified the use of the gray δ-Eddington formulation, Eq. (7), to approximate the phase function describing this highly forward scattering behavior

$$\Phi(\psi) = 2f\delta(1 - \cos\psi) + (1 - f)(1 + 3g\cos\psi) \quad (7)$$

where f and g quantify the forward scattering behavior and were specified to be 0.111 and 0.215, respectively. The Dirac-δ portion of Eq. (7) represents the forward spike in the phase function, or the fraction of scattering in the forward direction. The other portion represents the fraction scattered into other directions.

Monte Carlo Formulation

The Monte Carlo procedure as applied in this problem is a statistical method for predicting the radiative heat transfer by observing the results of a simulation. In this simulation, the histories of a number of energy bundles are tracked from emission through scattering, and ultimately to complete absorption within the medium and its surroundings. What happens to each of these bundles is dependent on the scattering and absorptive behavior within the medium. This behavior is modeled using a set of cumulative distribution functions (CDFs) which describe the probability of various events taking place. Specifically, in the current Monte Carlo formulation, CDFs are used to determine the direction and location of emission, the wave number of each bundle, the distance traveled between scattering events, and the direction of scatter. These CDFs are discussed in more detail below.

General Zonal Ray Tracing

The medium is divided into subregions, or volume elements, which are individually homogeneous in temperature, pressure, and particle concentration. The medium as a whole, however, can be inhomogeneous. The enclosure walls are divided into homogeneous subregions, or area elements. The number of bundles emitted from each subregion is based on the total emissive power of that subregion and the power per emitted bundle, a user-controlled number set at the beginning of the simulation. Calculation of the total emissive power is discussed below. In carrying out a simulation, each bundle emitted from within a given subregion is emitted following the completion of the history of the preceding bundle. After all bundles have been emitted from that subregion, the next subregion is processed. A given bundle's starting location within a subregion is determined randomly from a uniform distribution mapped to the geometry of the subregion by means of a finite element parametric mapping technique. The direction of emission from within a subregion in the medium is determined by Eqs. (8) and (9), described in Ref. 10:

$$\theta(R) = \arccos(1 - 2R) \tag{8}$$

$$\phi(R) = 2\pi R \tag{9}$$

Finally, for spectrally dependent media, the wave number of the energy bundle is determined as discussed below. Once this emission information is established, the bundle is ready to be tracked through the medium starting from within the emitting subregion.

The first step is to determine the radiative properties, namely, the spectral absorption, extinction coefficients, and the scattering albedo, for the subregion the bundle is currently traversing at the wave number for that bundle; this process is described below. Next, the point where the bundle would exit the subregion along its current direction and the distance, D_e, to that exit point are calculated. Then Eq. (10) is used to determine how far D the ray travels before it might be scattered[1]:

$$D = -(1/\kappa_\eta)\ln(R) \tag{10}$$

If the distance D is as large as D_e, the bundle will exit the current subregion at that exit location previously calculated. If not, then bundle's position is moved a distance D in its current direction and remains in the current subregion. In both cases a fraction of the bundle's current power is absorbed along the path traveled. This fraction is calculated by means of Eq. (11)

$$\text{Absorbed fraction} = 1 - e^{-\alpha S} \tag{11}$$

where S is set equal to the lesser of D or D_e. This absorbed power is subtracted from the bundle's currently existing power and added to the amount of power already absorbed by that subregion.

Next, if the bundle remained in the current subregion, the occurrence of scattering, or direction change, is determined by comparing a random number to the scattering albedo for the current subregion. If the random number is smaller than the albedo, the bundle's direction is changed. How the new scattered direction is established is discussed below. Once the energy absorbed has been recorded, the position updated, and the new direction established, the process, starting with exit-point determination, is repeated until the bundle leaves the current subregion or the bundle's energy level drops below a criterion set at simulation start. This criterion typically ranged from 0.1 to 0.001% of the power initially emitted in bundle. If a bundle's power level falls below this cutoff criterion, its history is terminated, its remaining power is added to the total absorbed power for the current subregion being traversed, and the next bundle is emitted from the appropriate subregion.

Once the bundle exits one subregion, the next subregion entered is automatically identified, radiative properties are determined for the new subregion, and the tracking procedure is reinitiated. This procedure is repeated for every subregion entered by a given bundle until that bundle's power level falls below the same predefined cutoff level or strikes an enclosure surface. If the bundle reaches an enclosure surface, it will be totally or partially absorbed depending on the absorptivity of that surface, and the absorbed power will be subtracted from the bundle's current power and added to the total for that surface. Partially absorbed bundles are reflected back into the neighboring subregion and the tracking process is continued. At present, only diffuse reflection and emission from enclosure walls are modeled.

To verify the tracking procedure, the heat flux values to the enclosure walls from a series of gray one- and three-dimensional media with different optical depths and scattering albedos were evaluated. Results were within 1% of analytical results.[11] In addition, the internal distribution of emissive power within a three-dimensional cube-shaped media with three hot enclosure walls was evaluated. Results were achieved which were within 1% of analytical results.[12]

The various results alluded to above were achieved using different values for the cutoff criterion and emitted power per bundle. Although detailed sensitivity numbers were not recorded, a few comments about the trends observed might be helpful. First, computer time was very sensitive to emitted-power-per-bundle in that decreases in this value resulted in inverse increases in the number of bundles tracked. For the above-mentioned internal distribution case, where a small grid size dictated a decreased power-per-bundle value, as many as 1,000,000 rays were tracked to obtain the high level of agreement with analytical results.

Second, although reducing the cutoff criterion from 0.1 to 0.001% did improve accuracy, reducing the cutoff criterion had only a minor impact on computer time, which seemed counterintuitive. For optically thin media, it was expected that a smaller cutoff criterion would allow the ray to travel longer distances and through more subregions, thus increasing the number of calculations and the computation time. However, this effect may have been mitigated by a decrease in the number of calculations along a given distance by virtue of the longer distances produced by Eq. (10), resulting in longer distances between calculations. Or it may have been that the optical depths of the individual subregions were too large to observe any major sensitivity. For optically thick media, power is absorbed so fast over a given distance that the distance required to absorb the extra power available in the longer-life bundle is minimal. Therefore, no change in computer time was expected or encountered for optically thick media. However, the combined effects of smaller grid sizes, optical depths, and reduced cutoff criterion have not been fully examined.

Spectral Modeling

Modeling the spectral behavior encompasses several key elements of this Monte Carlo procedure, including 1) determining the emissive power of a particular subregion, 2) selecting the wave number of a bundle being emitted, and 3) providing the wave number dependent absorption and scattering properties as the bundle history is being tracked through each subregion.

In this study, the emissive power[1] for each subregion with a different temperature, composition, or particle concentration is computed using Eq. (12) prior to each simulation

$$E = \alpha_p \sigma T^4 4 \, dV \tag{12}$$

where

$$\alpha_p = \frac{\int_0^{\eta=\eta^\infty} (\alpha_\eta + \alpha_{\eta c}) e_{b\eta} \, d\eta}{\sigma T^4} \tag{13}$$

The integral is evaluated by means of a trapezoidal rule with a uniform spectral increment between integration points. A uniform spectral increment was chosen to simplify programming and reduce user input. For inhomogeneous media, different nonuniform spacing would have been necessary for each subregion. The trapezoidal integration scheme was chosen for its simplicity and produced a synergism which facilitated the formation of the wave number CDF, discussed in more detail below, and which facilitated selection of radiative properties needed in the bundle tracking procedure.

In determining the proper integration range and increment, various ranges of η and different increments, $d\eta$, were used to perform the integration in an attempt to reach a converged α_p. Based on this procedure, η ranges from 400 to 10,000 cm^{-1}, with integration points every 5 cm^{-1}. This set of points is not intended to represent an optimum, nor is it capable of defining the line structure; it is only intended as a sufficient scheme for the purpose of capturing the model in Eqs. (3–6) for the media as specified in Ref. 7:

$$R(\eta) = \frac{\int_0^{\eta} (\alpha_\eta + \alpha_{\eta c}) e_{b\eta} \, d\eta}{\int_0^{\eta^\infty} (\alpha_\eta + \alpha_{\eta c}) e_{b\eta} \, d\eta} \tag{14}$$

As stated earlier, there is a synergism between calculating the emissive power and the wave number CDF which is derived from Eq. (14). As can easily be seen by comparing Eqs. (13) and (14), the denominator of Eq. (14), is computed when α_p is computed. In addition, since the integration is done in a piecewise fashion, the numerator is also computed during this same integration process. As each integration point is evaluated the numerator is computed and stored along with the corresponding η. Once the emissive power calculation is completed, the stored numerator values are normalized by the denominator; the result is a table for $R(\eta)$ with values at every 5 cm^{-1}. This table is then inverted to give $\eta(R)$, the CDF for determining the wave number of emission from the particular subregion being considered. The absorption and scattering coefficients corresponding to each η are also recorded in this table for subsequent use in the bundle tracking procedure. A similar table is built for every subregion with a different set of properties prior to the start of a simulation.

The accuracy of this procedure was verified by computing the enclosure heat flux for a series of media where the pressure, temperature, or the geometry was varied, and comparing the results with numerical results produced by an approach referred to as the sum of gray gases,[13] a curve fit approach based on Hottel's experimental data for carbon dioxide gas. The differences obtained ranged from less than 1–5%, which is within the numerical accuracy of either approach.

Scattering Model

As stated earlier in the media description, the phase function describing the anisotropic scattering produced by the carbon particles is approximated by means of Eq. (7) with the constants f and g specified in Ref. 7. ψ is the angle between the directions of the bundle prior to and after a scattering event.

In order to formulate the CDF used to select the direction of travel for a bundle following a scattering event, the phase function is altered to include only the directions different from the prescattering direction. In other words, the forward scattering spike, described by the Dirac-δ portion of the phase function, has been removed facilitating the integration required to produce the CDF. Consequently, the forward spike is not considered as scattering and its contribution to the scattering coefficient must be removed. This is accomplished by multiplying the spectral scattering coefficient, mentioned earlier, by the factor $(1 - f)$. The CDF representing the scattering direction is then derived by integrating the reduced phase function over the arbitrary range of solid angles, then dividing by the reduced phase function integrated over all solid angles. In addition, scattering is assumed to be azimuthally symmetric relative to the unscattered ray. Under these adjustments, the scattering direction CDF can be derived from Eq. (15)

$$R(\mu) = \frac{\int_{-1}^{\mu} (1 - f)(1 + 3g\mu) \, d\mu}{\int_{-1}^{1} (1 - f)(1 + 3g\mu) \, d\mu} \tag{15}$$

where

$$\mu = \cos(\psi) \tag{16}$$

Inverting the integrated result of Eq. (15) gives $\mu(R)$, the function for scattering direction in terms of R, Eq. (17):

$$\mu(R) = \frac{-1 + \sqrt{1 - 6g(2R - 1 - \frac{1}{3}g)}}{3g} \tag{17}$$

During the bundle tracking, if a scattering event takes place a random number is selected, and the cosine of the scattering angle is evaluated from Eq. (17). Next, the zenith angle relative to the original direction is determined directly and the azimuthal angle ϕ around the original direction is picked randomly from a uniform distribution of angles from 0 to 2π rad. Once the zenith and azimuthal angles and their direction cosines local to the original direction are determined, they are transformed to global coordinates for subsequent tracking.

Geometric Models

The present Monte Carlo algorithms were designed to accommodate arbitrary geometries composed of any number of parallelepiped subregions. This allows evaluation of radiative transfer within media having a wide variety of geometric configurations. The geometric and subregion information is modeled using I-deas,[14] a commercial finite element modeling package developed by SDRC. This information is then translated into the information needed by the Monte Carlo simulation routines. In addition to facilitating the modeling process for complex geometries, the use of finite element nodes and elements supports the search algorithms in the tracking routines, and offers the potential for automatically incorporating the radiative heat transfer results referenced to these nodes and elements into a multimode heat transfer analysis.

Results

The Monte Carlo simulations were performed for both the one- and three-dimensional geometries using a Silicon Graphics Indigo Workstation. Initially, a rudimentary investigation was made to determine how to obtain results with reasonable accuracy while maintaining minimal computer time. The most efficient way discovered to do this was to select lower values for emitted power per bundle (thus, higher numbers of emitted bundles per subregion), and decrease the number of simulations used to get an average. The following results for the complex media, previously described, were generated using an emitted power per bundle of 1 W. The results are discussed in three sections: 1) homogeneous media results, 2) inhomogeneous media results, and 3) comparison with other methods.

Homogeneous Media Results

Figure 3 shows the net radiative flux vs position for the one-dimensional media between two cold black surfaces, at the three different carbon concentrations levels and the two different total pressures, discussed previously. The zero location is the geometric center of the symmetric slab, at the plane of symmetry. The results indicate that the strong spectral-absorption-band structure for each medium plays a key role in determining the radiative heat transfer within the medium surrounded by cold walls.

Since the walls are cold, only the medium is considered to emit. Consequently, most of the emission occurs at wave numbers within the absorption bands of the carbon dioxide gas. This is controlled in the simulation by the wave number CDF. A typical wave number CDF is shown in Fig. 2 superimposed on the corresponding spectral absorption profile. The large increases in the CDF at the absorption bands, shown in Fig. 2, indicate the higher probability of emission within these bands, especially the asymmetric band at 2410 cm^{-1}. However, the high absorption within the center of these bands prevents the emitted bundles from traveling very far before they are completely absorbed. Consequently, the bundles contributing most to the heat transfer are those bundles with wave numbers on the fringe of or between the carbon dioxide absorption bands.

The addition of carbon particles appears to have three effects. The first of these is that as the concentration of carbon particles is increased, the wall heat flux increases. This is due to the increased emission of bundles in the windows between the strong carbon dioxide absorption bands, where absorption is small enough to allow the bundles to travel sufficient distances prior to termination. Second, for low and moderate concentrations, increasing the concentration has the effect of increasing the net radiative flux in the interior of the media.

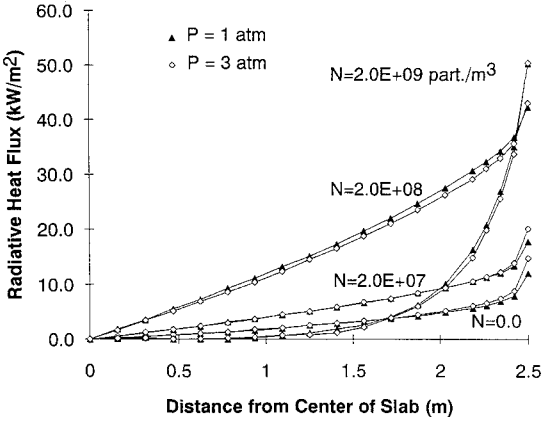

Fig. 3 Comparison of radiative heat flux through one-dimensional medium for a homogeneous medium at T = 1000 K, P = 1 or 3 atm (21% carbon dioxide, by volume), with N = 2.0E+07, 2.0E+08, or 2.0E+09 particles/m³.

At these concentrations, bundles with wave numbers in the windows can travel over several subregions enhancing the radiative transfer deep in the media. Third, for high concentrations, the absorption within the windows is so large that the bundles can travel only small distances. Consequently, only bundles emitted near the walls are significant for radiative transfer to the wall and internal net radiative transfer is minimal.

Increasing the pressure elevates the absorption and emission in the carbon dioxide, absorption bands which results in more bundles being emitted. However, the associated increase in absorption in the bands diminishes the effect resulting in no major change in the net radiative flux in interior regions shown in Fig. 3. Only a minor effect is observed for the case of moderate carbon particle concentration. However, the heat flux at the wall does increase slightly for the low carbon particle concentration case. These results indicate that the effect of increasing total pressure is negligible compared to the effect of increasing carbon particle concentration at higher concentrations.

To judge the variability of the one-dimensional results, the standard deviation for each flux value based on five separate simulations was calculated. For the case of high carbon particle concentration which exhibited the most variability, the typical standard deviation on any flux value was 200 W/m^2. The higher variability of this case is due to two factors. First, as the concentration increases to higher levels, the total absorption over the entire spectrum becomes quite high, severely limiting the distance each bundle may travel, even in the windows. Because of the limited distance, the number of bundles actually providing significant statistical radiative transfer information is reduced. Second, the increased scattering requires that more, not less, statistically significant bundles are needed to fully characterize the radiative transfer.

Figure 4 displays selected values of surface radiative flux and internal flux divergence calculated for the three-dimensional homogeneous media at three different carbon particle concentration levels under the conditions stated above in the media description. Figure 4a presents the radiative flux divergence vs location along the y axis, and Fig. 4b presents the surface flux values along the center of the wall in the x direction at $y = 0$ and $z = 1.5$ m. The flux divergence values are smallest in the middle of the medium and largest near the walls, similar to the one-dimensional results. This trend is primarily due to the boundary conditions of a specified hot temperature adjacent to a cold wall; the gas adjacent to the cold wall gives up more of its heat than gas in the interior. The corners of the medium exhibit even higher divergence values, as there are two walls to heat. However, the surface heat flux near the corners is reduced because there is less media able to radiate to them.

Figure 4a also shows a multidimensional effect. Based on the one-dimensional results, it is expected that the flux divergence values in the interior regions for the high carbon particle concentration case would be lower than those values for either of the other two cases. However, the low carbon particle concentration case had the lowest flux divergence in the medium interior. This is possibly because the radiative flux can now leave the interior in all directions, not just in one direction. The absorption within the spectral fringes and windows for the low concentration case is lower than that for the high concentration case, therefore, the loss of energy from the center regions into the other directions is greater for the low concentration case.

Typical standard deviations in the results for the three-dimensional media for the low-, moderate-, and high-particle concentration cases were, respectively, 225, 320, and 400 W/m^2 for flux values, and 1250, 1730, and 2850 W/m^3 for flux divergence values. These variability values were based on two separate simulations. Higher variability was observed in areas of large gradients, especially in flux divergence. Since this

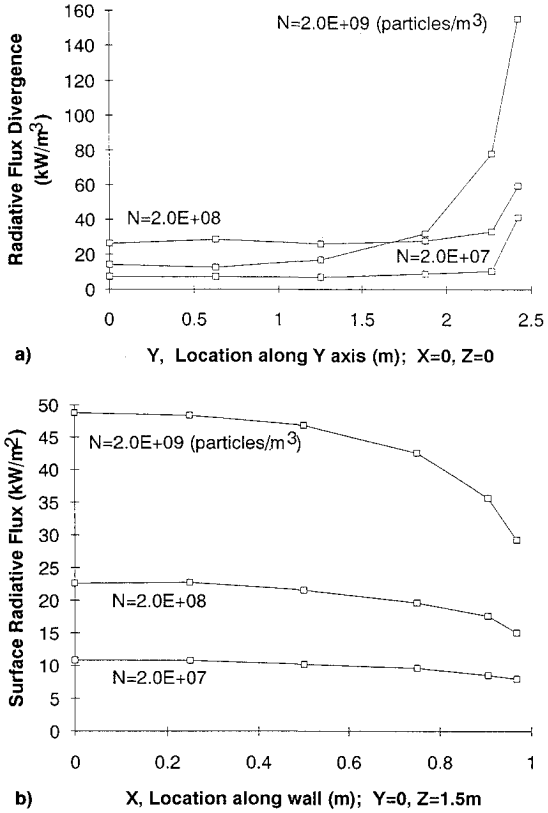

Fig. 4 a) Comparison of radiative flux divergence at $Y = 0$ and $Z = 0$ and b) comparison of surface radiative flux at $Y = 0$ and $Z = 1.5$ m for a homogeneous medium at $T = 1000$ K, $P = 1$ atm (21% carbon dioxide, by volume), with $N = 2.0E+07$, $2.0E+08$, or $2.0E+09$ particles/m^3.

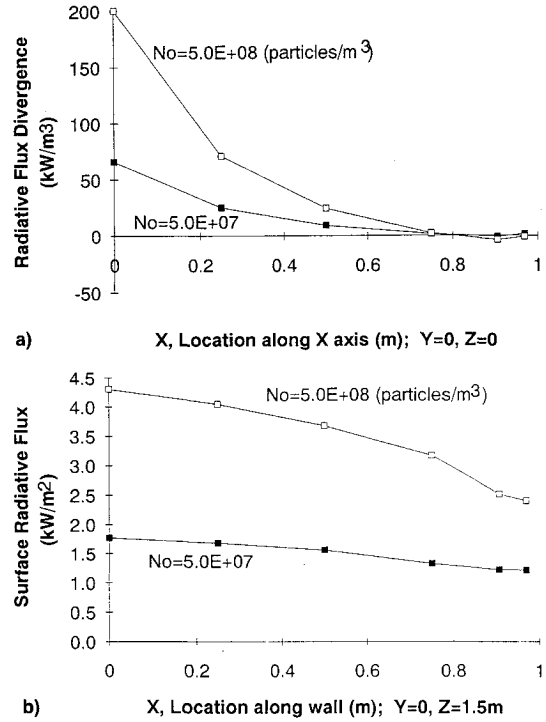

Fig. 5 a) Comparison of radiative flux divergence at $Y = 0$ and $Z = 0$ and b) comparison of surface radiative flux at $Y = 0$ and $Z = 1.5$ m for an inhomogeneous medium with $T_0 = 500$ K, $P = 1$ atm (21% carbon dioxide, by volume), and $N_0 = 5.0E+07$ or $5.0E+08$ particles/m^3.

process determines flux divergence for finite subregions, there tends to be some grid size dependence in the flux divergence as well as increased variability. In addition, calculating the flux divergence for only finite subregions limits the determination of flux divergence near the wall. An alternate approach for determining the flux divergence based on incident flux is currently under development. However, since the discretized approach was used for this article, the sizes of the subregions near the wall were reduced so that the divergence values calculated for subregions near the wall would approach the divergence at the wall. This also allows better characterization of the gradients near the wall. However, a limiting consideration regarding this shrinking approach is that the number of rays emitted reduces as the subregions are shrunk leading to increased variability. Investigation is currently underway to solve this shortcoming.

Inhomogeneous Media Results

Figure 5 presents selected surface flux and internal flux divergence results for the inhomogeneous media for two different carbon particle concentration cases. Figure 5a presents the radiative flux divergence vs location along the x axis, and Fig. 5b shows the surface flux along the center of the wall in the x direction at $y = 0$ and $z = 1.5$ m. The behavior of the flux divergence is opposite that from the homogeneous cases. Flux divergence values are quite high in the center region where both the temperature and carbon particle concentration are the highest and fall off toward the wall. In fact, for both cases the flux divergence near the x walls (which bound the shortest dimension) falls below zero, indicating these regions are acting as energy sinks rather than sources. The low temperature near the wall reduces the emission in these regions, while the reflection of radiative heating from the nonblack walls plus emission from hotter interior regions increase the power entering these outer regions. The same phenomenon occurs near the other walls, but to a lesser degree due to their longer distances from the center. The surface flux distributions for the inhomogeneous cases resemble those for the homogeneous cases. The larger flux values occur in the middle of each face due to radiative transfer with more of the media. Conversely, corner walls receive less heating, being exposed to less of the media. Adding more carbon particles to the media has the same effect as seen in the one-dimensional results; the increased particle concentration produced elevated wall heat flux.

The typical standard deviations for the surface flux results were 70 W/m^2 and 100 W/m^2 for the low and moderate particle concentration cases, respectively. The standard deviations for the flux divergence results were, typically, 700 W/m^3 and 1000 W/m^3, for the two cases, respectively. These values were determined based on five separate simulations. Based on both the homogeneous and inhomogeneous variability numbers, the size of the standard deviations appears to be dependent on the emissive power of the media; the larger the emissive power the higher the variability. However, when normalized by the emissive power of the media, the percent deviation decreases. This tends to support the idea that using more bundles to characterize the behavior of the media improves the relative accuracy of that characterization.

Comparison with Other Methods

The results obtained by this Monte Carlo procedure are compared to selected results obtained by other methods discussed at the symposium.[7] Shown in Fig. 6 are comparisons of selected surface radiative flux results obtained by three methods: 1) the current Monte Carlo method, 2) a Monte Carlo method developed by Yuen,[15] and 3) a YIX method.[16] Noticeable differences are observed between the results produced by the different methods. Gray results, with and without scattering, obtained since the symposium by each method compared very well—within a few percent. This suggests that the differences between the results may be attributable to

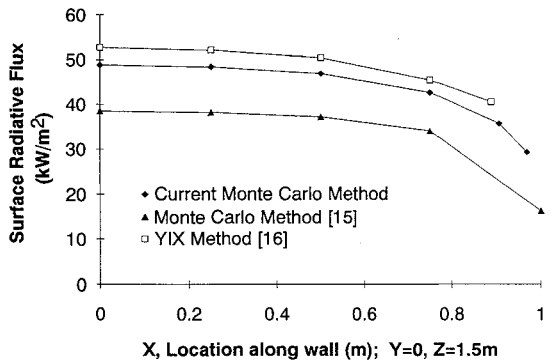

Fig. 6 Comparison of surface radiative flux at $Y = 0$ and $Z = 1.5$ m for a homogeneous medium at $T = 1000$ K, $P = 1$ atm (21% carbon dioxide, by volume), with $N = 2.0E+09$ particles/m^3, calculated by three different methods.

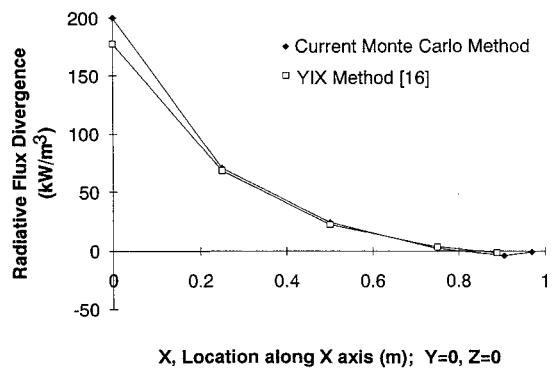

Fig. 7 Comparison of radiative flux divergence at $Y = 0$ and $Z = 0$ for an inhomogeneous medium with $T_0 = 500$ K, $P = 1$ atm (21% carbon dioxide, by volume), and $N_0 = 5.0E+08$ particles/m^3, calculated by two methods.

differences in the spectral model implementations. Investigations into what specifically caused these differences is still ongoing and is focused toward the spectral model details, such as number of spectral bands or integration scheme. Figure 7 presents the flux divergence along the x axis for the inhomogeneous moderate concentration case discussed above. Results obtained by the current Monte Carlo method and the YIX method are shown. The disagreement in the results in the center regions is due primarily to the grid size difference. Subsequent Monte Carlo simulations, performed with smaller grid sizes in the center regions, have confirmed this.

Conclusions

A Monte Carlo method has been developed and applied to predict the radiative transfer within a medium containing anisotropically scattering particles and a highly spectral gas. The Monte Carlo method is described, and the formulation of the cumulative distribution functions, which influence the events in a simulation, particularly the spectral absorption and anisotropic scattering behavior, are discussed. The geometric modeling and bundle tracking procedures were developed for a general three-dimensional inhomogeneous medium and have been applied to both one- and three-dimensional geometries and the accuracy and sensitivities of the method have been briefly discussed.

The radiative transfer in media exhibiting both highly spectral absorption and emission and anisotropic scattering has been evaluated. Both homogeneous and inhomogeneous media have been modeled. Results for the one-dimensional media indicate that elevated pressure has only a limited effect on radiative heat transfer, over the pressure range studied (1–3 atm), when compared to the effects of elevated carbon particle concentrations. One- and three-dimensional results indicate that increased carbon particle concentration can significantly increase radiative flux received by the enclosure surrounding the media, and can either depress or increase the radiative flux divergence deep within the media depending on particle concentration levels. Results for the inhomogeneous media evaluations demonstrate the strong temperature dependence of the radiative flux and flux divergence and the effect of a reflective wall on the flux divergence near the wall.

This Monte Carlo procedure is shown to be suitable for this type of problem and appears to be adaptable with minimal effort to a wide range of media and geometries. Accuracies for surface radiative flux were typically greater than those for radiative flux divergence profiles within the media. On the computer system used in this study, CPU time is long even for the simplest of geometries, when detailed profile data are calculated. However, this process appears to be appropriate to massively parallel processing which would greatly reduce the time required for solution. Subsequent plans call for the development of parallelized algorithms and implementation on multiprocessor computers.

References

[1]Siegel, R., and Howell, J. R., *Thermal Radiation Heat Transfer*, 2nd ed., Hemisphere, New York, 1982, pp. 354–382, 751–767.

[2]Haji-Sheikh, A., "Monte Carlo Methods," *Handbook of Numerical Heat Transfer*, Wiley, New York, 1988.

[3]Lewis, E. E., and Miller, W. F., Jr., *Computational Methods of Neutron Transport*, Wiley, New York, 1984, pp. 296–360.

[4]Modest, M. F., "The Monte Carlo Method Applied to Gases with Spectral Line Structure," *Developments in Radiative Heat Transfer*, American Society of Mechanical Engineers HTD-Vol. 203, 1992, pp. 79–84.

[5]Subramaniam, S., and Mengüc, M. P., "Solution of the Inverse Radiation Problem for Inhomogeneous and Anisotropically Scattering Media Using a Monte Carlo Technique," *International Journal of Heat and Mass Transfer*, Vol. 34, No. 1, 1991, pp. 253–266.

[6]Mengüc, M. P., and Viskanta, R., "Radiative Transfer in Three Dimensional Rectangular Enclosures Containing Inhomogeneous, Anisotropically Scattering Media," *Journal of Quantitative Spectroscopy and Radiative Transfer*, Vol. 33, No. 6, 1985, pp. 533–549.

[7]Tong, T. W., and Skocypec, R. D., "Summary on Comparison of Radiative Heat Transfer Solutions for a Specified Problem," *Developments in Radiative Heat Transfer*, American Society of Mechanical Engineers HTD-Vol. 203, 1992, pp. 253–258.

[8]Edwards, D. K., Glassen, L. K., Hauser, W. C., and Tuchscher, J. S., "Radiation Heat Transfer in Nonisothermal Nongray Gases," *Journal of Heat Transfer*, Vol. 89, No. 3, 1967, pp. 219–229.

[9]Foster, P. J., and Howarth, C. R., "Optical Constants of Carbon and Coals in the Infrared," *Carbon*, Vol. 6, No. 5, 1968, pp. 719–729.

[10]Taniguchi, H., "The Radiative Heat Transfer of a Gas in a Three Dimensional System Calculated by Monte Carlo Method," *Bulletin of the Japan Society of Mechanical Engineers*, Vol. 12, No. 49, 1969, pp. 67–78.

[11]Siegel, R., "Transient Radiative Cooling of a Droplet-Filled Layer," *Journal of Heat Transfer*, Vol. 109, No. 1, 1987, pp. 159–164.

[12]Tan, Z., "Radiative Transfer in Multidimensional Emitting, Absorbing, and Anisotropic Scattering Media—Mathematical Formulation and Numerical Method," *Journal of Heat Transfer*, Vol. 111, No. 1, 1989, pp. 141–147.

[13]Farag, I., "Non-Luminous Gas Radiation: Approximate Emissivity Models," *Proceedings of the Seventh International Heat Transfer Conference*, Munchen, Germany, Vol. 2, 1982, pp. 487–492.

[14]Anon., "SDRC I-deas Finite Element Modeling User's Guide," Structural Dynamics Research Corp., Millford, OH, 1990.

[15]Yuen, W. W., Ma, A. K., and Takara, E. E., "Evaluation of Radiative Heat Transfer Using the Generalized Zonal Method and the Absorption Mean Beam Length Concept," *Developments in Radiative Heat Transfer*, American Society of Mechanical Engineers HTD-Vol. 203, 1992, pp. 265–273.

[16]Hsu, P., Tan, Z., and Howell, J. R., "Application of the YIX Method to Radiative Heat Transfer Within a Mixture of Highly Anisotropic Scattering Particles and Non-Gray Gas," *Developments in Radiative Heat Transfer*, American Society of Mechanical Engineers HTD-Vol. 203, 1992, pp. 285–300.